HNUE JOURNAL OF SCIENCE DOI: 10.18173/2354-1059.2021-0030
Natural Sciences 2021, Volume 66, Issue 2, pp. 75-82
This paper is available online at http://stdb.hnue.edu.vn

# MOLECULAR DYNAMICS SIMULATIONS OF MECHANICAL PROPERTIES OF CuNi ALLOYS UNDER PRESSURE

Pham Thi Lien[1], Thieu Thi Thu[2], Dinh Cong Thanh[2] and Nguyen Thi Thao[2]
[1]*Faculty of Basic Sciences, University of Economics - Technology for Industries*
[2]*Faculty of Physics, Hanoi National University of Education*

**Abstract.** Structural characterization of CuNi alloys during the cooling process at different pressures from 0 GPa to 45 GPa is performed by Molecular dynamics (MD) simulations. The interaction potential used in the calculations for interactions between different types of atoms in the sample is the Quantum Sutton-Chen embedded potential. The increase of the pressure increases crystal-forming temperature. Mechanical properties of these samples at 300 K and different pressures were determined by using the mechanical analysis. The Young modulus of these models increases with the increase of pressure. During the deformation process, the number of disorder atoms increases dramatically in the elastic region and unchanged in the plastic region. Sliding deformation is recognized at different pressure under tensile deformation.

***Keywords:*** CuNi alloys, deformation, shear band.

## 1. Introduction

Mechanical properties and deformation mechanisms are important properties of materials that affect their applicability. Therefore, the study of mechanical properties of materials plays an important role in guiding the fabrication as well as measures to improve the durability of materials. There are many research works on the mechanical properties of alloys, including CuNi alloys because of their special properties [1-4]. The mechanical properties of CuNi alloys depend on the concentration of Cu and Ni atoms in the sample. With the increase of Ni concentration in the sample, the ultimate tensile strength and yield strength of samples increasing [1]. As the Cu concentration increases, the value of the elastic modulus decreases [5]. For nanocrystalline materials prepared by gas condensation or vacuum consolidation, the decrease in elastic or shear modulus is explained by the porosity of the material [6]. The studies related to the plastic deformation mechanism of Cu metal or Cu alloys with the face-centered cubic structure

Received June 2, 2021. Revised June 17, 2021. Accepted June 24, 2021.
Contact Nguyen Thi Thao, e-mail address: thaont@hnue.edu.vn

were conducted under different uniaxial deformation methods [7-8]. Structural features of these alloys during the annealing or the cooling process depend on the pressure of the models [9, 10]. During the annealing process, when the pressure of samples is increased, the incubation time of the crystallization is longer and the crystallization process becomes slower. However, there are few studies on the influence of pressure on the mechanical properties of CuNi alloys, especially at high pressure.

In this study, the mechanical properties of Cu-Ni alloys with different pressures will be studied through uniaxial deformation, focusing on analyzing void distribution in the sample and calculating the shear modulus at different strains.

## 2. Content

### 2.1. Computational methods

The simulation model has the size of 8788 atoms (Cu:Ni = 8:2). The interaction potentials of atoms of the system are quantum Sutton-Chen (Q-SC) embedded potential given by Ref. [11]. The Q-SC potential leads to accurate values for vacancy energies, surface energies, and stacking-fault energies. The sample is heated to 2000 K to break the original random structure at different pressure of 0 GPa, 10 GPa, 20 GPa, 30 GPa, and 45 GPa. These samples are then cooled down to 300 K at the cooling rate of 0.01 K/ps.

The effect of pressure on the structural and mechanical characteristics of these samples during the cooling process and at a temperature of 300 K was analyzed through potential energy (PE), CNA (The Common Neighbor Analysis) methods, and tensile deformations.

Perform tensile strain on the samples at 300 K with a strain rate of 0.512/ps. The method of performing the deformation is detailed in the previous work [12]. The atomic local shear strain calculations $\eta_i^{\text{Mises}}$ for each atom i give information about the plastic deformation of the sample [13]. $\eta_i^{\text{Mises}}$ is used to determine the degree of local deformation at the atom i. The equation for $\eta_i^{\text{Mises}}$ is as follows:

$$\eta_i^{\text{Mises}} = \sqrt{\eta_{xy}^2 + \eta_{xz}^2 + \eta_{yz}^2 + \frac{\left(\left[\eta_{xx} - \eta_{yy}\right]^2 + \left[\eta_{xx} - \eta_{zz}\right]^2 + \left[\eta_{yy} - \eta_{zz}\right]^2\right)}{6}}$$

where $\eta_{xy}, \eta_{xz}, \eta_{yz}$ are the shear components and $\eta_{xx}, \eta_{yy}, \eta_{zz}$ are the normal components of the strain at the atom i. This quantity is widely used to determine the formation of shear transformation zones (STZs) and shear bands (SBs) in amorphous materials [14-16].

### 2.2. Results and discussions

The samples were cooled to 300 K from 2000 K with a cooling rate of 0.01 K/ps with different pressures. Figure 1 shows the dependence on temperature of potential energy (PE) of samples. During the cooling process, the atomic potential energy of the samples gradually decreased, there existed a range of temperature where the atomic

potential energy dropped suddenly at pressures of 45, 30, 20, and 10 GPa. At a pressure of 0 GPa there is no sudden change in atomic potential energy. From the graph of energy-dependent temperature, we can determine that the range of transition temperature decreases with the decrease of pressure. The ranges of transition temperature corresponding to the considered pressures from 45 GPa to 10 GPa are 1150 - 1320 K, 1100 - 950 K, 950 - 850 K, and 800 - 500 K.

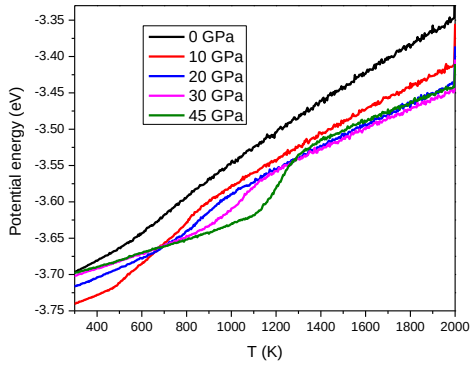


***Figure 1. The potential energy as a function of temperature under the cooling process at different pressures***

After the cooling process, we analyze the effect of pressure on the structure as well as the mechanical properties of samples at 300 K and different pressures.

The structure of the samples at different pressures was specifically analyzed through the radial distribution functions (RDFs) and the number of atoms in the samples shown in Figure 2. The RDF of the sample at 0 GPa represents the structure of the amorphous sample. At all different pressures, the samples exhibit the RDFs of the crystal structure. The types of crystal atoms formed in the sample are face-centered cubic (fcc) and the hexagonal close-packed *(*hcp*)* phases. The number of different types of atoms is shown in Figure 2b. At the pressure of 0 GPa, the number of amorphous atoms is the greatest, while at the remaining pressures that paper investigates this value is very small. This result is consistent with the analytical results of PE and RDFs.

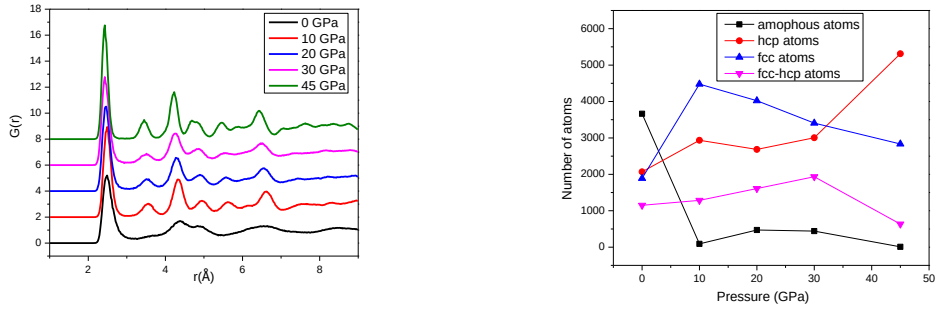


a) b)

***Figure 2. The total RDF of $Cu_{80}Ni_{20}$ samples (Figure 2a) and the change of number of different types of atoms as a function of pressure at 300 K (Figure 2b)***

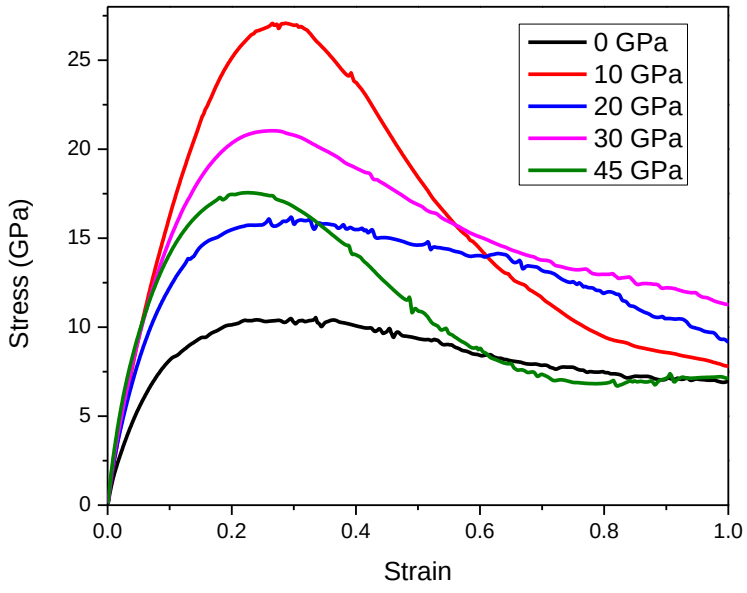


***Figure 3. The stress-strain curve of samples at 300 K under uniaxial tension at different pressures***

The mechanical properties of the samples were analyzed by applied uniaxial tension tests. The stress-strain curves of samples at different pressures are indicated in Figure 3. One can see that the stress increases linearly to the maximum value then decrease to saturation value at all pressures. This proves that all samples have both elastic deformation region and plastic deformation upon tension test. The values of Young's modulus are calculated from the slopes of the stress-strain curves in the linear region as shown in Table 1. This value increases with increasing pressure. This result is in good agreement with the results identified by reference [5].

***Table 1. Pressure dependence of the elastic modulus of $Cu_{80}Ni_{20}$ alloy samples***

| **Pressure (Gpa)** | 0 | 10 | 20 | 30 | 45 |
|---|---|---|---|---|---|
| **Elastic modulus (GPa)** | 145 | 203 | 229 | 271 | 291 |

The variation of the number of different types of atoms during deformation is shown in Figure 4. During the deformation, the number of disordered atoms increases suddenly while the number of crystalline atoms decreases suddenly in the plastic region and unchanged in the elastic region.

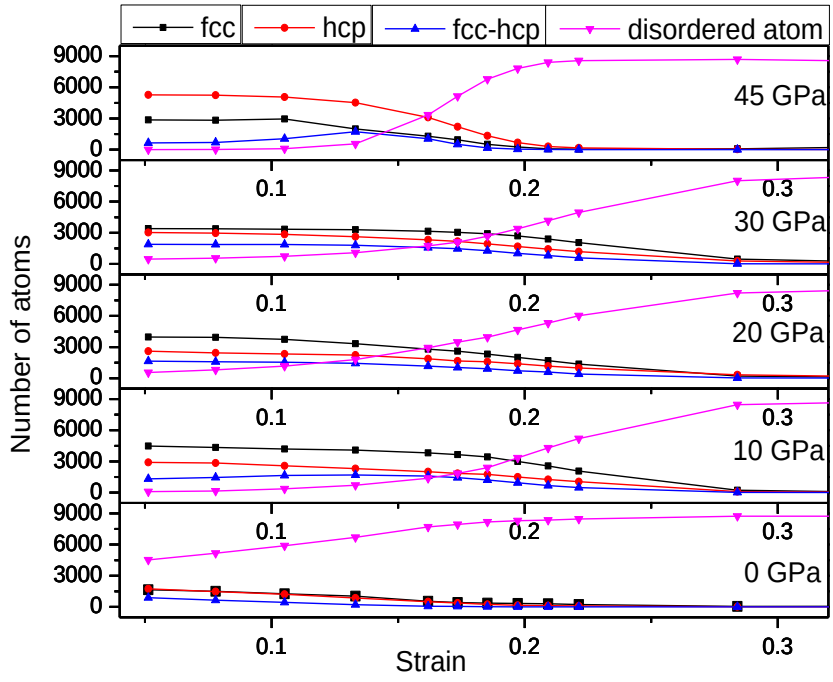


***Figure 4. Variations of fcc, hcp, hcp-fcc, and amorphous atoms under uniaxial tension process at different pressures***

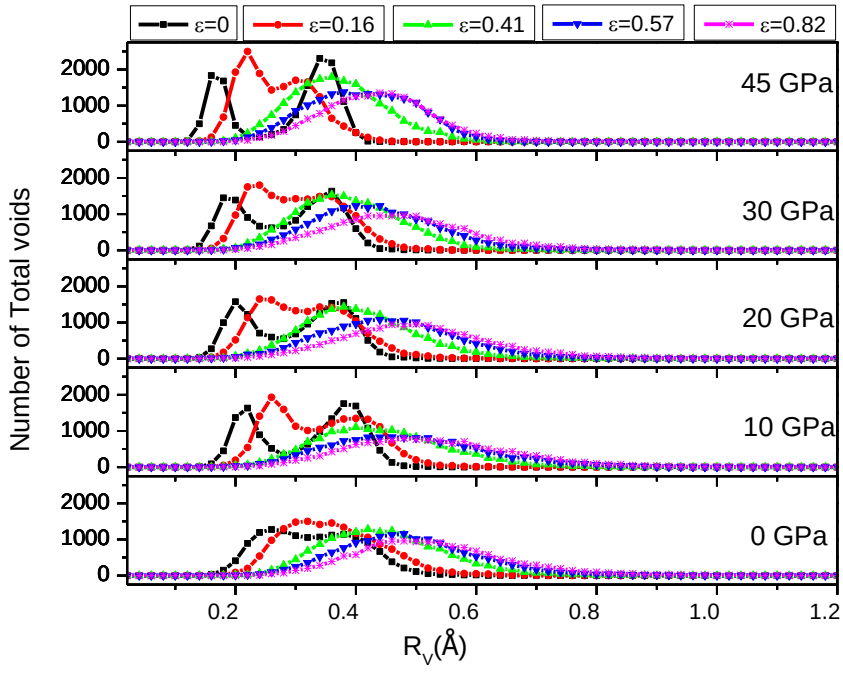


***Figure 5. The distributions of total voids by radius during uniaxial tension***

The porosity of CuNi alloys can be examined through the analysis of voids. The distributions of the total voids (RDVs) by radius under uniaxial tension are shown in Figure 5. One can see that the peaks of these RDVs move gradually to the right and become expand when strain increases. This proves that the radius of these voids increases with increasing strain.

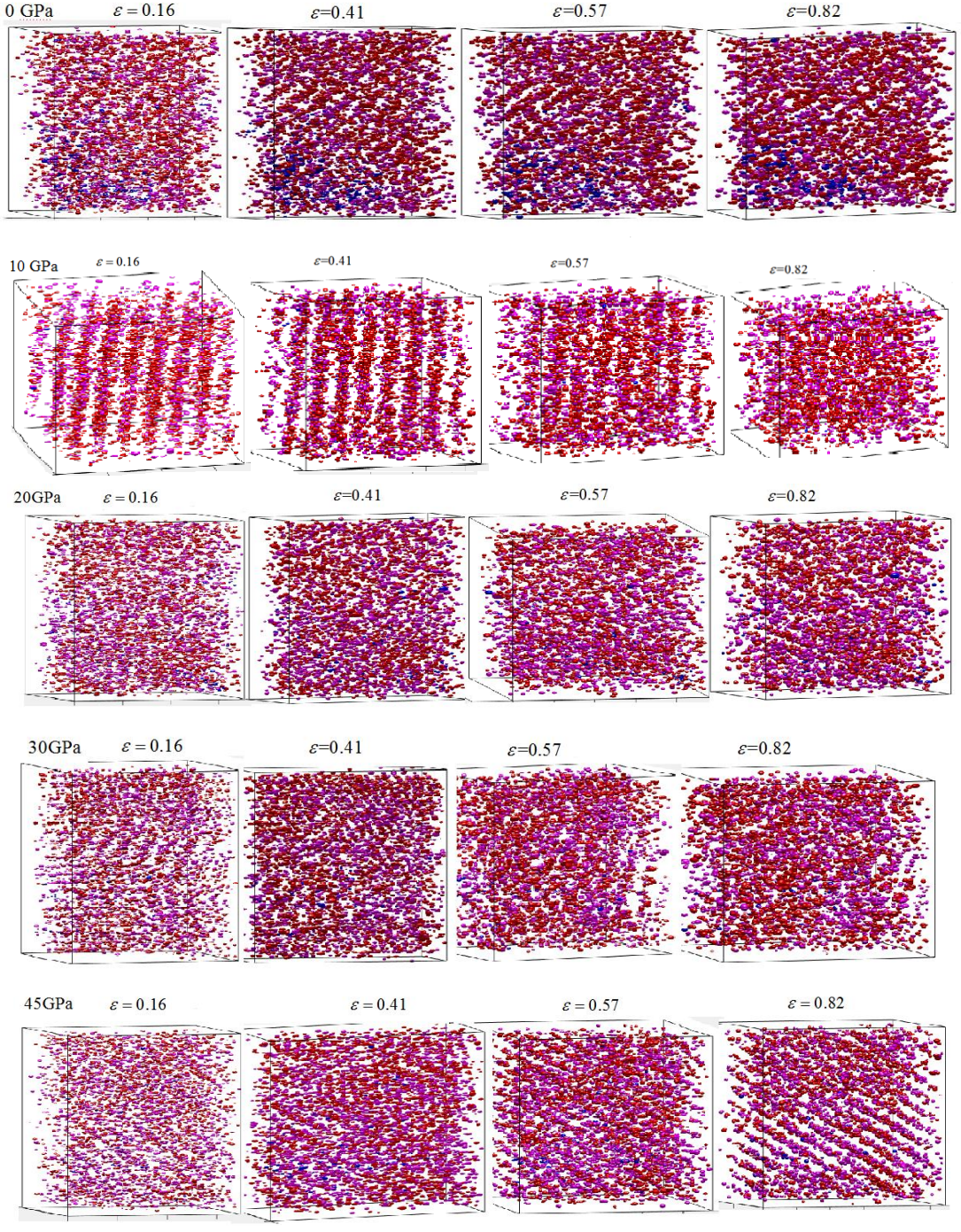


***Figure 6. Visualization of voids in the samples during tensile deformation***

Figure 6 shows the image of voids in the samples under tensile deformation. Here Cu-void is defined as contacting with Cu and Cu atoms and no Ni atom. Similarly, the Ni-void contacts with Ni and Ni atoms and no Cu atom while the Cu-Ni-void contacts with Cu and Ni atoms. These visualizations show that the number of big voids increases as strain increases. The same type of voids tend to form clusters and are arranged in planes. This allows the shear deformations to occur which will be observed below.

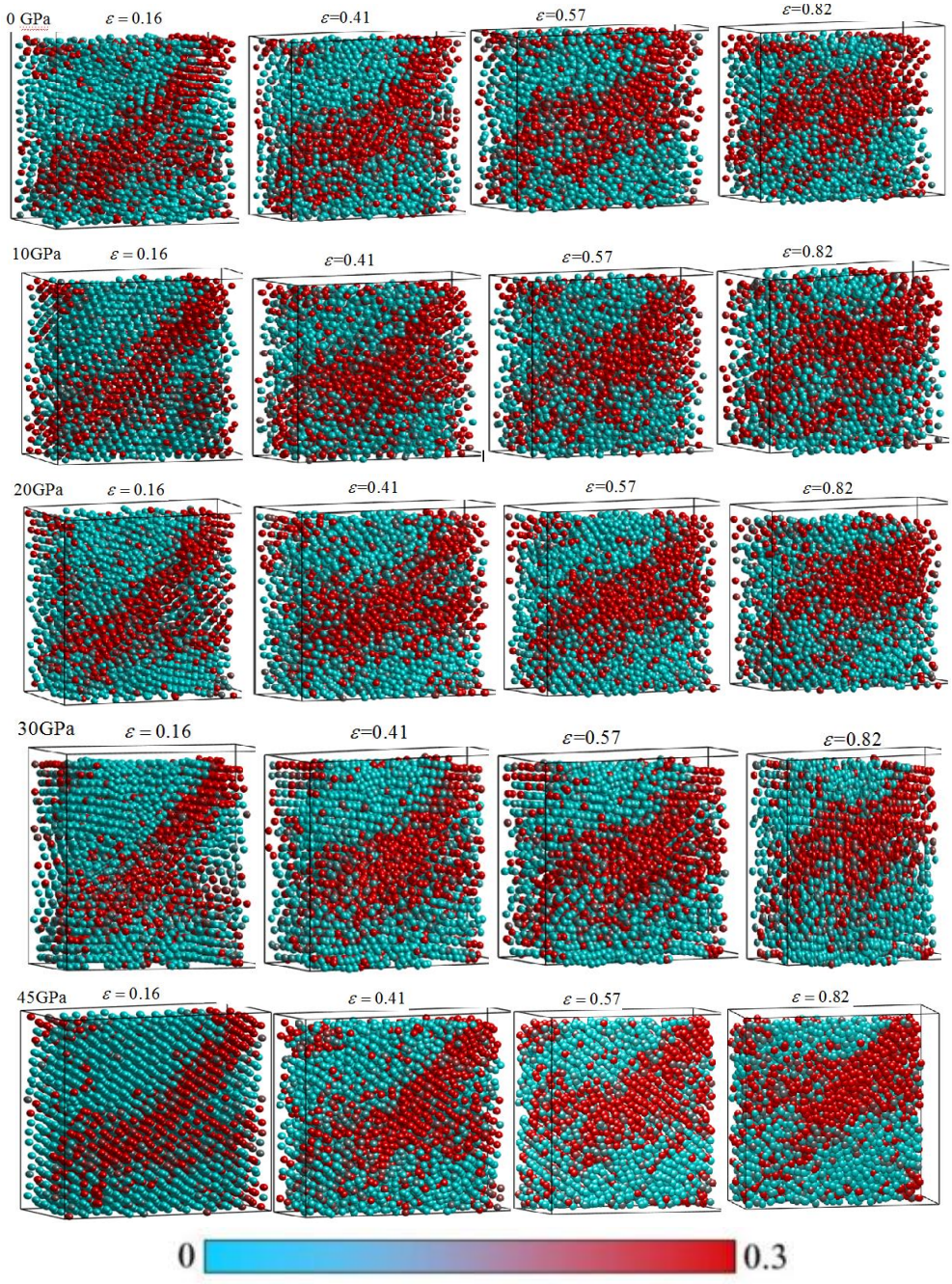


***Figure 7. Sliding deformation of atoms are visualized according to their atomic shear strain calculated with*** $\Delta\varepsilon = 0.006$ ***at different pressures***

The plastic strain concentration was calculated by the atomic local shear strain, $\eta_i^{Mises}$. Here a large value of $\eta_i^{Mises}$ represent that atom *i* perform shear deformation, whereas a small one shows that atom *i* make a small displacement relative to all its neighboring atoms. Figure 7 shows atoms with the value of $\eta_i^{Mises}$, which was calculated with $\Delta\varepsilon = 0.006$ between the current and reference configurations. One can see that the formation of SBs may occur at all strains and pressures. These SBs propagate at the direction ~45$^o$ from the tensile direction.

## 3. Conclusions

CuNi alloy samples at 300 K which were cooled from 2000 K at the cooling rate of 0.01 K/ps, were analyzed for structural and mechanical properties at different pressures by molecular dynamic simulations. The structure of the samples at 300 K depends on the pressure, the total number of crystalline atoms is greatest at the pressure of 45 GPa, and at 0 GPa the number of disordered atoms is the largest. The values of Young's modulus increase with increasing pressure. The radii of voids in the samples increase with increasing strain. Shear bands are observed at all pressures during strain.

***Acknowledgments.*** This work is supported by the Vietnam Ministry of Education and Training under Grant Number B2020-SPH-01.

## REFERENCES

[1] Z.Y. Wang, D. Han, X.W. Li, 2017. *Materials Science & Engineering* A, 679, 484.
[2] W. Li, S. Lu, Q.M. Hu, K. Kwon, B. Johansson, L. Vitos, 2014. *J. Phys-Condens. Mat*., 26, 277.
[3] K. Nakajima, K. Numakura, 1965. *Phil. Mag.*, 12, 361.
[4] S. Lu, Q.M. Hu, E.K. Delczeg-Czirjak, B. Johansson, L. Vitos, 2012. *Acta Mater*, 60, 4506.
[5] T.D. Shen, C.C.Koch, T.Y.Tsui and G.M.Pharr, 1995. *J. Mater. Res.*, Vol. 10, No. 11, 2892.
[6] V.Krstic, U. Erb, and G. Palumbo, 1993. *Scripta Metall. Mater.*, 29, 1501.
[7] X.W. Li, N. Peng, X.M. Wu, Z.G. Wang, 2014. *Metall. Mater. Trans*. A, 45, 3835.
[8] Y.Z. Tian, L.J. Zhao, S. Chen, A. Shibata, Z.F. Zhang, N. Tsuji, 2015. *Sci. Rep.* 5, 23.
[9] S. Kazanc, 2007. *Physics letter* A, 365, 473
[10] Nguyen Thi Thao and Trinh Thi Thu Hang, 2020. *HNUE Journal of Science, Natural Sciences*, Volume 65, Issue 6, p. 54.
[11] Yue Qi, Tahir Cagin, Yoshitaka Kimura, and William A.Goddard III, 1998. *Physical review* B, 59, 5, 3527.
[12] V.V.Le, T.T.Nguyen, K.H.Pham, 2013. *J. Non-Crystal. Solids*, 363, 6.
[13] F. Shimizu, S. Ogata, J. Li, 2007. *Mater. Trans.*, 48, 2923.
[14] Y. Zhao, X. Peng, T. Fu, C. Huang, H. Xiang, N. Hu, C. Yan, 2018. *Materialia*, 2, 148.
[15] S. Feng, L. Qi, L. Wang, S. Pan, M. Ma, X. Zhang, G. Li, R. Liu, 2015. *Acta Materialia*, 95, 236.
[16] A.J. Cao, Y.Q. Cheng, E. Ma, 2009. *Acta Materialia*, 57, 5146.